Sports Eng
DOI 10.1007/s12283-014-0158-y

ORIGINAL ARTICLE

Numerical simulations of the frictional collisions of solid balls on a rough surface

S. Mathavan · M. R. Jackson · R. M. Parkin

Abstract Three-dimensional simulations of the frictional collision between solid balls moving on a rough surface are analyzed in this paper. The analysis is performed in the context of pool and snooker, two popular games in the pocket billiards family. Accurate simulations of ball motion in billiard games are useful for television broadcasts, training systems and any robotic game playing systems. Studying solid ball collisions in a three-dimensional space requires careful consideration of the different phenomena involved in ball motion such as rolling, sliding and ball spin about a general axis. A set of differential equations are derived describing ball dynamics during collisions. In the absence of explicit analytical solutions to the differential equations, a numerical procedure is performed to determine post-collision ball velocities and spins after collision. In addition, the paper also presents a methodology to analyze the curved, slip trajectories of balls immediately after impact. The results presented here, when compared with some experimental shots, show that the percentile errors in post-collision velocities are reduced by the proposed method. The prediction accuracies for ball travel direction are increased twofold by the proposed impact simulation algorithm.

Keywords Impulse with friction · Frictional impact · Solid balls · Billiards · Snooker · Pool · Massè

S. Mathavan (✉)
ASML Netherlands BV, De Run 6501, 5504, DR, Veldhoven, The Netherlands
e-mail: s.mathavan@ieee.org

M. R. Jackson · R. M. Parkin
Intelligent Automation Research Group, Wolfson School of Mechanical and Manufacturing Engineering, Loughborough University, Loughborough LE11 3UZ, UK

Published online: 03 June 2014

List of symbols

e	Coefficient of restitution between the balls
F	Force
I	Moment of inertia of the balls
M	Mass of the balls
N	Number of iterations
P	Accumulated impulse at any time during impact
P_I^c	Accumulated impulse at the termination of compression
P_I^f	The final accumulated value of impulse
R	Radius of the balls
s	Slip speed between the balls
s'	Slip speed between the cue ball and the table
s''	Slip speed between the object ball and the table
V_0	Incident speed of the ball
W	Work done due to impulse force
x	Ball position on the table along the X-axis
y	Ball position on the table along the X-axis
z	Ball position on the table along the X-axis
ΔP	Impulse during a time of Δt
θ	The angle that the common normal of the ball–cushion contact point makes with the horizontal
μ_{bb}	Coefficient of sliding friction between the balls
μ_s	Coefficient of sliding friction between the ball and cushion
Φ	Direction of slip between the balls
Φ'	Direction of slip between the cue ball and the table
Φ''	Direction of slip between the object ball and the table
ω	Angular speed of the ball
ω_0^T	Topspin of the ball at incidence
ω_0^S	Sidespin of the ball at incidence
$\dot{\omega}_r$	Resistance of the table surface to ball sidespin

Superscripts

C Cue ball

O Object ball

Subscripts

G Parameters measured about ball centroid
I Along normal impulse between the balls
n Iteration number of numerical simulation
N Common normal at the point of contact between the balls and the table (for forces)
N_f Terminal iteration number of numerical simulation
R Along the surface at the point of contact between the balls and the table (for frictional forces)
S At the end of the slipping phase of a ball

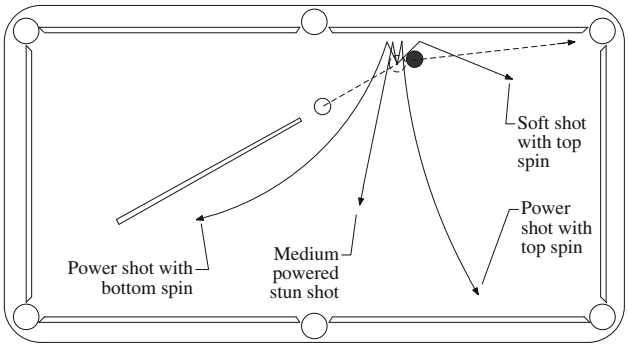

Fig. 1 Resulting cue ball locations after a ball-pot for different topspin and sidespin imparted on the cue ball [16]

1 Introduction

Snooker is a cue sport belonging to the pockets billiards family. Another related, popular game is pool. Since the physical and dynamical phenomena involved in both these games are exactly the same, billiard physics and billiard dynamics are usually employed to refer to these. In addition, when referring to both games together, the common terms 'pocket billiards' or simply 'billiards' are used throughout this text. The games uniquely combine a high level of strategic play and superior physical skill. Interest in snooker has grown steadily in the last few years with an exponential growth found in the Far East. Almost half of the UK's population watched the World Championship on the BBC in 2011 with as much as 3.9 million people watching a single session, whereas the Chinese television station CCTV5 reported viewing figures as high as 30 million [1]. Pool is an equally popular game, consisting of a number of variants such as eight-ball, which is very played very commonly in the United States.

Pocket billiards has always been associated with physics due to the classical nature of concepts such as friction and collision, associated with it. It is important to note that the earliest associated literature is found as early as 1,835 [2]. A number of publications on billiards dynamics have been published in the last two decades, e.g., Salazar and Sanchez-Lavega [3], de la Torre Juárez [4] and Cross [5, 6]. In addition, recent research has concentrated on robotic billiards playing systems [7–10], trainer-assistance systems [11–13], and on the development of strategies for game play [14]. In this context, the work described in this paper is part of a research effort to develop a robotic manipulator for snooker [15]. Each of these three sets of systems described above has the need to analyze various available shots, for a given table state and select the best next shot available. The ability to impart different spins and velocities to the cue ball in combination with some exquisite collision dynamics present between balls results in a variety of ball trajectories giving the players a high level of flexibility (see Fig. 1).

Nowadays, a vast number of online virtual snooker games are available, e.g., Snooker Skool from Yahoo! Games. Although most of the online games simulate snooker in 2D, 3-dimensional versions are also found [17]. In addition, the TV broadcasts make use of ball tracking systems such as HawkEye [18] that also simulate and predict ball behavior. Accurate ball collision simulations will make these virtual games and predictions more realistic.

Traditionally, ball collisions have been analyzed without incorporating the effect of friction, and the object ball is supposed to move along the line connecting the ball centers at the instant of impact [19]. A comprehensive review of the existing literature shows that there are two categories of collision models for billiards. The first ones do not take ball spin into account in the analysis of ball–ball collisions at all. The works of de la Torre Juárez [4] and Wallace and Schroeder [20] belong to this category. Three other works, Marlow [21], Kondic [22] and Domenech [23], consider the effect of ball spin. Marlow [21] highlights the effects of ball spin, but has not proposed a collision model. The work of Kondic [22] is limited as it only treats the case of head-on collisions. Domenech [23] provides a detailed study of billiard ball collisions. The paper clearly identifies the tangential impulse components, which are present due to the 3D spins of the balls, under different possible scenarios at the interfaces between the balls and between the balls and the table, e.g., unidirectional slips and different stick–slip regimes. For each of the situations, analytical solutions have been given. Moreover, the paper considers the case of the cue ball under pure rolling, and no sidespin, colliding with an object ball, and identifies the evolution of different regimes, based on stick and sliding, at the different material interfaces during impact. However, it fails to identify the evolution of different regimes for a general impact, e.g., one that involves various levels of top or bottom spin and

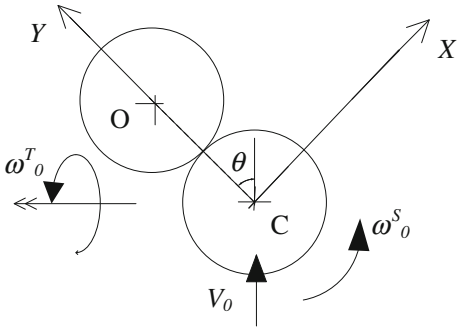

Fig. 2 A general oblique impact between balls (ω_0^T direction is given by the right-hand grip rule)

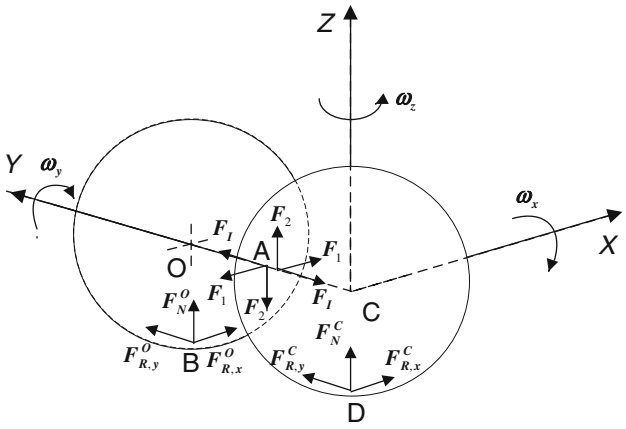

Fig. 3 The forces acting on the balls during the impact

sidespin, thereby not being able to predict analytical solutions for post-collision ball velocities and angles.

The forgoing literature summary on ball collisions indicates that there are no generalized collision models available, involving ball spin, that can be applied to any given shot in snooker. In the absence of such a model, the best complete model that can predict a given shot is given by Wallace and Schroeder [20]. It was shown, in Mathavan et al. [24], that there are errors, of up to 6°, in the directions of post-collision ball motion predicted by the model of Wallace and Schroeder [20]. This amount of angular uncertainty is sufficient enough to allow an object ball, which is as close as 200 mm to a pocket before the collision, to miss the pocket by a distance of 20 mm. The resulting effect on the cue ball is equally harmful, due to the unexpected exit angle after collision, as it may end up in a totally different position on the table. As potting accuracy and precisely predicting final cue ball positions after a shot is of paramount importance in pocket billiards, the high deviation between the actual and predicted ball trajectories will affect the accuracy of the simulated game play. Therefore, analysis is required regarding the very general impact between snooker or billiards balls to provide realistic simulations.

In the following analysis, initially, a general solution will be derived for the problem of two identical balls colliding obliquely, and at the end, the values applicable for snooker will be substituted. Here, the problem of the cue ball, C, obliquely impinging on to another object ball O is analyzed (see Fig. 2). Both the cue and object balls are assumed to have equal mass and radius. In Fig. 2, it is important to note that ball C does not spin about its frontal axis (about the direction of V_0), this condition is only prevalent during a massé shot and is not normally encountered in snooker.

When two spheres collide, a contact is made over a finite size of area on their surface, due to the deformation present at the interface. The contact area between the spheres during impact is usually estimated through the Hertz theory. However, a point contact is assumed here. The assumption of a point contact has also been used by other researchers such as Kondic [22] and Domenech [23].

In this paper, collisions between two snooker balls are studied using the principles of impact mechanics. The next section describes theoretical derivations. Simulation results are subsequently presented and discussed extensively, followed by a conclusion section.

2 Theory

The balls are assumed to be moving on a flat surface; hence, the point of their contact will be at a height of R from the surface. This is depicted in Fig. 3.

2.1 General equations of motion

In Fig. 3, for ball C, for the linear motion along X, Y and Z directions

$$F_1 + F_{R,x}^C = M\ddot{x}_G^C \tag{1a}$$

$$-F_I + F_{R,y}^C = M\ddot{y}_G^C \tag{1b}$$

$$F_2 + F_N^C - mg = M\ddot{z}_G^C \tag{1c}$$

Here, F denotes the instantaneous normal force acting on any of the points of contact between the balls and the table interface, as shown in Fig. 3. In Eq. (1a), superscripts denote the sphere to which a particular parameter belongs to. The subscript G stands for the centroid values of a sphere. Thus, $\ddot{z}_G^C$ denotes the centroid acceleration of C along the Z-axis.

By considering an infinitesimal time period of Δt, the increment and the accumulated impulse values can be expressed as,

$$\Delta P = \int_{t}^{t+\Delta t} F \cdot \mathrm{d}t \tag{2a}$$

and,

$$P = \sum \Delta P = \int_{0}^{t} F \cdot \mathrm{d}t \tag{2b}$$

The impulse–momentum change relationship along the above directions result in the following equations.

For cue ball C, at time t, consider an increment Δt in time, from Eqs. (1a) and (2a)

$$\Delta P_1 + \Delta P_x^C = M\left[\dot{x}_G^C(t+\Delta t) - \dot{x}_G^C(t)\right] \tag{3a}$$

$$-\Delta P_I + \Delta P_y^C = M\left[\dot{y}_G^C(t+\Delta t) - \dot{y}_G^C(t)\right] \tag{3b}$$

$$\Delta P_2 + \Delta P_N^C = M\left[\dot{z}_G^C(t+\Delta t) - \dot{z}_G^C(t)\right] \tag{3c}$$

It should be noted that in Eq. (3c), the impact component due to gravity acting on the ball, mg, is absent. de la Juarez [4] suggests that in the limit $\Delta t \to 0$, non-diverging forces, such as those due to gravity, will have a negligible contribution on momentum changes.

Moment of impulse and angular momentum about the center of mass for ball C about X, Y and Z directions are given by,

$$\left(\Delta P_2 + \Delta P_y^C\right)R = \frac{2MR^2}{5}\left[\omega_x^C(t+\Delta t) - \omega_x^C(t)\right] \tag{3d}$$

$$-\Delta P_x^C R = \frac{2MR^2}{5}\left[\omega_y^C(t+\Delta t) - \omega_y^C(t)\right] \tag{3e}$$

$$-\Delta P_1 R = \frac{2MR^2}{5}\left[\omega_z^C(t+\Delta t) - \omega_z^C(t)\right] \tag{3f}$$

Similar sets of equations can also be derived for ball O. The impulse change of momentum equations equivalent to (3) will be

$$-\Delta P_1 + \Delta P_x^O = M\left[\dot{x}_G^O(t+\Delta t) - \dot{x}_G^O(t)\right] \tag{4}$$

Five other equations, similar to (3b)–(3f) above, can be written for the object ball as well. Due to space restrictions, they are omitted here.

2.2 Impact dynamics

At the contact point of the balls, A, relative to ball O, let that ball C has a relative speed $s(t)$ at angle $\Phi(t)$ with the X-axis (the relative velocity vector will lie on the XZ plane). The instantaneous value of the normal impulse P_I (the accumulated value of all ΔP_Is until time t), which is always positive within the interval of impact, monotonously increases with time; thus, in this analysis, it is taken as an independent variable, instead of the usual variable of time t [25]. Slip speeds along the X and Z axes, respectively, are as follows:

$$\dot{x}_A = \dot{x}_A^C - \dot{x}_A^O = s(P_I)\cos(\Phi(P_I)) \tag{5a}$$

$$\dot{z}_A = \dot{z}_A^C - \dot{z}_A^O = s(P_I)\sin(\Phi(P_I)) \tag{5b}$$

The normal component of relative velocity,

$$\dot{y}_A = \dot{y}_A^C - \dot{y}_A^O = \dot{y}_G^C - \dot{y}_G^O \tag{5c}$$

For the nominal slipping speeds to be along the positive X and Z axes, when the balls are sliding on each other at their contact point A, from the Amontons-Coulomb law,

$$\Delta P_1 = -\mu_{bb}\cos(\Phi(P_I))\Delta P_I \tag{6a}$$

$$\Delta P_2 = -\mu_{bb}\sin(\Phi(P_I))\Delta P_I \tag{6b}$$

where μ_{bb} is the coefficient of sliding friction between the balls.

Notably, depending on the value of vertical sliding velocity between the balls, i.e., $\dot{z}_A$ as given in Eq. (5b), some of the impulses in the equation sets (3a) or (4) will be zero. If $\dot{z}_A$ is negative, ball C will have more downward velocity (along the Z-axis) at the contact point A, and the frictional impulse along Z, ΔP_2, between the balls will be acting on the balls in the directions as shown in Fig. 3. This condition is given by,

$$\Delta P_2 > 0 \tag{6c}$$

If ball C is to remain on the table, from Eq. (3c),

$$\Delta P_2 + \Delta P_N^C < 0 \tag{6d}$$

The conditions in (6c) and (6d) can only be satisfied when,

$$\Delta P_N^C < 0 \tag{6e}$$

and apparently, it is impossible to satisfy the condition in (6e) as the table cannot apply a 'negative' reaction on the ball. Thus,

$$\Delta P_N^C = 0 \tag{6f}$$

Condition (6c) in turn says that the associated frictional impulses are also absent, i.e.,

$$\Delta P_x^C = 0 \text{ and } \Delta P_y^C = 0 \tag{6g}$$

Here, ball C will lift up from the table, like the cue ball in a 'jump' shot; Kondic [22] and Domenech [23] also acknowledge this effect. However, it is assumed in this paper that during the time of the impulse, it remains at the same spatial location, just above the table, without altering the geometrical configuration presented in Fig. 3. This assumption is reasonable since the time of impulse between two balls is very small and is in the range of 0.3 ms [21].

Conversely, if $\dot{z}_A$ is positive, then,

$$\Delta P_N^O = 0,\ \Delta P_x^O = 0 \text{ and } \Delta P_y^O = 0 \tag{6h}$$

Finally, if $\dot{z}_A$ is zero,

$$\Delta P_2 = 0 \tag{6i}$$

When (6i) prevails, both the balls will be either in contact with the table or airborne. Hence,

$$\Delta P_N^C = \Delta P_N^O = 0 \tag{6j}$$

and the associated friction components will also be zero.

If ball C is touching the table at any instant during impact, to satisfy the condition, $\dot{z}_G^C(t+\Delta t) - \dot{z}_G^C(t) = 0$ and from (3c)

$$\Delta P_N^C = -\Delta P_2 = \mu_{bb} \sin(\Phi(P_I))\Delta P_I \tag{7a}$$

Else, if ball O is on the table, to satisfy the condition,

$$\dot{z}_G^O(t+\Delta t) - \dot{z}_G^O(t) = 0$$

it can be shown that

$$\Delta P_N^O = \Delta P_2 = -\mu_{bb} \sin(\Phi(P_I))\Delta P_I \tag{7b}$$

If ball C touches the table at point D with the table plane, slip s' and slip angle Φ' with the X-axis (s' will lie on the XY plane), and from (7a), for the sliding condition,

$$\begin{aligned}\Delta P_x^C &= -\mu_s \cos(\Phi'(P_I))\Delta P_N^C \\ &= -\mu_{bb}\mu_s \sin(\Phi(P_I)) \cos(\Phi'(P_I))\Delta P_I\end{aligned} \tag{8a}$$

Similar expressions can be derived for along the Y-axis and those for ball O along X and Y involving slip s'' and slip angle Φ'' with the X-axis (s'' will be on the XY plane). Let these be denoted by (8b)–(8d).

Here, μ_s is the sliding friction coefficient between the balls and the table. Sliding speeds are

$$\dot{x}_D = \dot{x}_D^C = s'(P_I)\cos(\Phi'(P_I)) \tag{9a}$$

$$\dot{y}_D = \dot{y}_D^C = s'(P_I)\sin(\Phi'(P_I)) \tag{9b}$$

Or

$$\dot{x}_B = \dot{x}_B^O = s''(P_I)\cos(\Phi''(P_I)) \tag{9c}$$

$$\dot{y}_B = \dot{y}_B^O = s''(P_I)\sin(\Phi''(P_I)) \tag{9d}$$

Hereafter, the practice of having the independent variable P_I with the dependent variables is dropped to keep the equations compact, e.g., $s'(P_I)$ this is simply written as s'.

2.2.1 Conditions for rolling

When rolling occurs, slip speed s (or s' and s' for the sliding on the table) becomes zero. At this instance, the relative motion between bodies stops at their contact point along the common tangent. The frictional forces become null.

1. When there is no slip between the balls (i.e., $s = 0$), which is a common occurrence depending on the initial conditions, as shall be seen shortly, where both the spheres will be rolling on each other at their contact point A.

   $$\Delta P_1 = \Delta P_2 = 0$$

   consequently,

   $$\Delta P_N^O = \Delta P_x^O = \Delta P_y^O = 0$$

2. When $s' = 0$, $\Delta P_x^C = \Delta P_y^C = 0$ and ball C will roll on the plane without sliding.
3. When $s'' = 0$, $\Delta P_x^O = \Delta P_y^O = 0$ and ball O will roll on the plane without sliding.

2.2.2 Coefficient of restitution

According to Stronge [25], the energetic coefficient of restitution e, is independent of friction and the process of slip. e^2 is the negative of the ratio of the work done by the impulse force during the restitution phase to that during the compression phase. Let P_I^f, P_I^c denote the accumulated impulse at the termination of impulse and at the end of compression, respectively. Then, it is possible to show that the work done is

$$\Delta W_y = \int F_I.\dot{y}_A \mathrm{d}t = \int \dot{y}_A \mathrm{d}P_I \tag{10a}$$

The coefficient of restitution is given by,

$$e^2 = \frac{-\int_{P_I^c}^{P_I^f} \dot{y}_A \mathrm{d}P_I}{\int_0^{P_I^c} \dot{y}_A \mathrm{d}P_I} \tag{10b}$$

This can be rearranged as,

$$W_y\left(P_I^f\right) = \left(1 - e^2\right) W_y\left(P_I^c\right) \tag{10c}$$

The termination of compression occurs when the normal component of relative velocity becomes zero, i.e.,

$$\dot{y}_A\left(P_I^c\right) = 0 \tag{10d}$$

2.3 Velocity relationships

The velocity of any point on a sphere's surface can be written with respect to its centroidal velocity, in vectorial notation as,

$$\vec{\mathbf{V}} = \vec{\mathbf{V}}_G + \vec{\omega}\Lambda\vec{\mathbf{R}} \tag{11a}$$

At contact point A

$$\dot{x}_A^C = \dot{x}_G^C - R\omega_z^C, \dot{z}_A^C = \dot{z}_G^C + R\omega_x^C, \dot{x}_A^O = \dot{x}_G^O + R\omega_z^O \text{ and } \dot{z}_A^O = \dot{z}_G^O - R\omega_x^O \tag{11b}$$

Similar expressions can be derived at D and B for the cue and object ball, respectively.

Using

$$\Delta\vec{\mathbf{V}} = \Delta\vec{\mathbf{V}}_G + \Delta\vec{\omega} \times \vec{\mathbf{R}} \tag{11c}$$

the finite difference counterparts of these equations are as follows:

$$\Delta\dot{x}_A^C = \Delta\dot{x}_G^C - R\Delta\omega_z^C, \Delta\dot{z}_A^C = \Delta\dot{z}_G^C + R\Delta\omega_x^C, \Delta\dot{x}_A^O = \Delta\dot{x}_G^O + R\Delta\omega_z^O \text{ and } \Delta\dot{z}_A^O = \Delta\dot{z}_G^O - R\Delta\omega_x^O \tag{11d}$$

$$\Delta\dot{x}_D^C = \Delta\dot{x}_G^C - R\Delta\omega_y^C \text{ and } \Delta\dot{y}_D^C = \Delta\dot{y}_G^C + R\Delta\omega_x^C \tag{11e}$$

$$\Delta\dot{x}_B^O = \Delta\dot{x}_G^O - R\Delta\omega_y^O \text{ and } \Delta\dot{y}_B^O = \Delta\dot{y}_G^O + R\Delta\omega_x^O \tag{11f}$$

2.4 Solution for the ball velocities

Using the expression in the previous sections, and depending on which ball is airborne (i.e., whether $\Delta P_C^O = 0$ or, i.e., $\Delta P_N^O = 0$), two sets of 12 differential equations (DEs) can be derived. Moreover, another set of 12 DEs can be expressed for the condition of $\Delta P_2 = 0$, where both the balls stay on the table or both are airborne. None of these 3 sets of DEs have exact solutions. A numerical solution is still possible. For example, for the problem of rotating spheres colliding into each other in free space, Kane and Levinson [26] have used a numerical scheme to obtain the variation of the sliding velocities, etc., during the time of impact, for both the spheres. A numerical solution is sought in this paper additionally.

The work done during an increment of the normal impulse between the balls, ΔP_I, must also be calculated numerically, using Eq. (10a),

$$\left(W_y\right)_{n+1} - \left(W_y\right)_n = \Delta P_I \frac{\left[\left(\dot{y}_A\right)_{n+1} + \left(\dot{y}_A\right)_n\right]}{2} \tag{12}$$

See Sect. 2.4.3 on the explanation on the numerical scheme employed.

2.4.1 Initial conditions

When $P_I = 0$, the centroidal velocities of ball C,

$$\left(\dot{x}_G^C\right)_1 = V_0 \sin\theta, \left(\dot{y}_G^C\right)_1 = V_0 \cos\theta, \left(\dot{z}_G^C\right)_1 = 0, \tag{13a}$$

with the rotational speeds being,

$$\left(\omega_x^C\right)_1 = -\omega_0^T \cos\theta, \left(\omega_y^C\right)_1 = \omega_0^T \sin\theta, \left(\omega_z^C\right)_1 = \omega_0^S. \tag{13b}$$

For ball O, the centroidal velocities are as follows:

$$\left(\dot{x}_G^O\right)_1 = 0, \left(\dot{y}_G^O\right)_1 = 0, \left(\dot{z}_G^O\right)_1 = 0, \left(\omega_x^O\right)_1 = 0, \left(\omega_y^O\right)_1 = 0, \left(\omega_z^O\right)_1 = 0. \tag{13c}$$

Also,

$$s(0) = \left|\sqrt{\left(V_0 \sin\theta - R\omega_0^S\right)^2 + \left(R\omega_0^T \cos\theta\right)^2}\right| \text{ and } \Phi(0) = \tan^{-1}\left(-\frac{R\omega_0^T \cos\theta}{V_0 \sin\theta - R\omega_0^S}\right) \tag{13d}$$

Between ball O and the table,

$$s'(0) = 0. \tag{13e}$$

Between ball C and the table,

$$s''(0) = \left|V_0 - R\omega_0^T\right| \text{ and } \Phi''(0) = 0. \tag{13f}$$

2.4.2 The values of friction and restitution coefficients

Here, the values of the friction coefficients between the balls, μ_{bb}, and that between the balls and the table, μ_s, and the coefficient of restitution between the ball, e, are determined. The authors determined the sliding coefficient of friction between the balls and table (μ_s) in snooker as between 0.178 and 0.245; see [24]. The average value of 0.21 for μ_s is used for simulations. The values for μ_{bb} and e parameters presented in the literature are vague. Only Marlow [21] has been found to report about these. Marlow predicts a value of 0.06 for μ_{bb} for well-polished balls. Furthermore, when the balls have any foreign material, such as chalk, on their surface, according to Marlow μ_{bb} may be as high as 0.2. Contradictorily, a variation of μ_{bb} in the form of,

$$\mu_{bb} = 9.951 \times 10^{-3} + 0.108e^{-1.088s}$$

is also put forward by Marlow [21], where s denotes the slip speed between the balls. The experimental process in obtaining the aforesaid variation did not seem reliable enough. According to Marlow, e is greater than 0.92. It is believed that the high speed camera measurements taken by these authors, and partly described in Mathavan et al. [24], are far superior to the techniques used by Marlow [21], and these results are used for the calculations and simulations performed.

The experimental plot shown in Fig. 4 is used in conjunction with these numerical simulations to obtain the values of the coefficient of restitution and the value of sliding friction. The fundamental idea is to replicate the experimental results by numerical simulations, using two random numerical values for the above parameters by a trial-and-error procedure. The experimental plot shown in Fig. 4 was obtained under the conditions of cut angle (θ), sidespin (ω_0^S) and topspin (ω_0^T) assuming the values of, 0°,

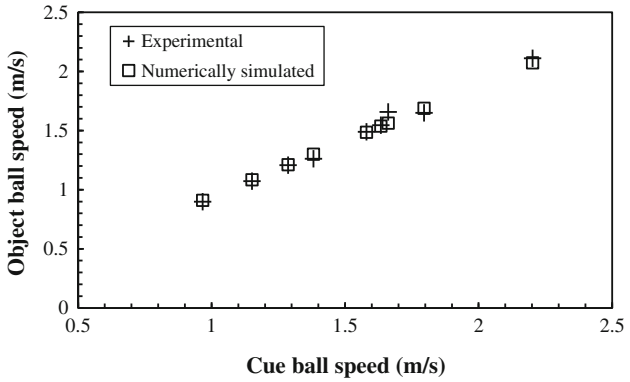

Fig. 4 Experimental results and numerical predictions for $\mu_{bb} = 0.05$ and $e = 0.89$ and under the conditions of $\theta = 0°, \omega_0^S = 0$, and $\omega_0^T = \frac{V_0}{R}$

0 and $\frac{V_0}{R}$, respectively (see Fig. 2). For each of the incident speed values, V_0, given in Fig. 4, the value of centroid velocity of the object ball at the termination of impact, $\dot{y}_G^O\left(P_I^f\right)$, was found numerically for the restitution coefficient between the balls, e, in the range 0.7–1.0 and the friction coefficient (μ_{bb}) between 0 and 0.2, both in 0.01 increments. For given values of friction and restitution coefficients between the balls, i.e., μ_{bb} and e, the RMS value of all the errors between the experimental and the numerical values for each of the incident velocities given in Fig. 4 was obtained. The values of a ball–ball friction value (μ_{bb}) of 0.05 and a restitution coefficient (e) of 0.89 were found to have the least RMS error value. The agreement of these values with Marlow's [21] values of 0.06 and 0.92 should be noted. Figure 4 also includes the numerically predicated results for a μ_{bb} of 0.05 and an e of 0.89.

2.4.3 *Numerical algorithm*

For snooker balls, the mass, M, and radius, R, are 0.1406 kg and 26.25 mm, respectively. The numerical scheme is written in MATLAB® programming language. The values of initial cue ball velocities (V_0, ω_0^T, ω_0^S) and the angle of collision, θ, are the inputs to the scheme. The smaller the value of the increment in the normal impulse between the balls P_I, i.e., ΔP_I, which is chosen as the independent variable for this problem, the more accurate the results will be. The aim is to find the centroid velocities of the balls at the final accumulated impulse value P_I^f.

In order to assume a reasonable value for increment of the normal impulse between the balls, ΔP_I, to start the numerical scheme, an approximate value for P_I^f can be taken as $(1+e)MV_0\cos\theta$, which is the value of the impulse had ball O been a solid wall. Hence, for N iterations,

$$\Delta P_I = \frac{(1+e)MV_0\cos\theta}{N} \tag{14}$$

Clearly, the values of final and end of compression phase impulse values (P_I^c and P_I^f) will decide the actual number of iterations that have taken place in the scheme.

For each iteration of the scheme, the state of the balls is determined at contact points A, B and D, i.e., it is determined whether they are in the state of rolling or sliding, which balls are airborne, etc. For this purpose, the equations Sect. 2.2 are used. Then, for each increase of ΔP_I, i.e., normal impulse between the balls, the code initially starts by calculating the increments in the impulses that determine the changes in velocity components for both the balls; equation sets (3) and (4) are used. Consequently, velocity increments are estimated followed by the determination of new ball velocities, both linear and rotational. The increment in work done is also estimated using Eq. (12). Now, state of motion at points A, B and D are evaluated and the scheme is continued until the normal relative velocity between the balls, $\dot{y}_A$—as in Eq. (5c)—becomes negative, i.e., the termination of the compression phase. The work done up to this iteration is $W_y\left(P_I^c\right)$. Equation (10c) is used to determine $W_y\left(P_I^f\right)$. The numerical algorithm is stopped when,

$$W = W_y\left(P_I^f\right). \tag{15}$$

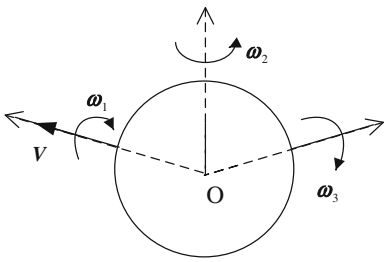

Fig. 5 A ball that spins about its frontal velocity axis

2.5 Parabolic path subsequent to impact

Execution of the numerical scheme that is described in Sect. 2.4.2 shows that, in general, both the cue ball and the object ball will have spins about their frontal velocity axes, as shown in Fig. 5. The ball shown in Fig. 5 has a spin component of ω_1 about its centroid velocity V. In this case, irrespective of the other two spin components, the ball will move along a curved path. This is called massé in billiards [21]. Curved shots can be made by elevating the cue when striking the ball. Curved ball trajectories are also produced due to frictional percussions during the impact between two balls or that between a ball and a cushion. The second

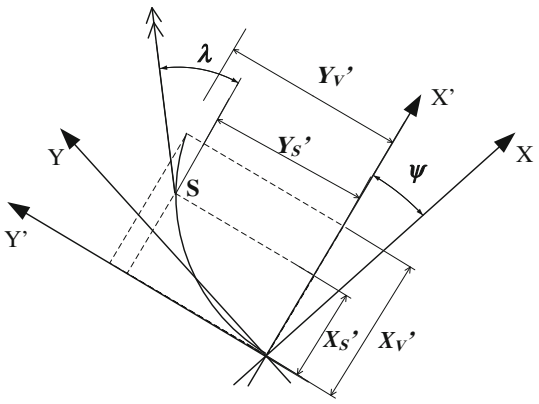

Fig. 6 Curved path of object ball O

type is of interest here. However, the derivations given in this section are, essentially, applicable for any general curved shot.

Here, the example of the object ball O is used to derive, with appropriate symbols, the description of trajectory of the ball under the massé conditions. The effect of table friction will generally impart a spin about the velocity axis of the object ball, as in a spinning bullet. This will curve the path of ball O immediately after the termination of impact, making the final direction of movement different to that at the termination of impulse. Its effect will be very prominent for high values of μ_{bb}. In mathematical terms, at the termination of impact, when n is equal to N_f, the final step of the numerical algorithm, this condition for curving is created when

$$\Phi'_{N_f} = \beta_{N_f} \tag{16}$$

Here β_{N_f} denotes the direction of its velocity of the center of gravity of ball O (i.e.,), given by

$$\tan\beta_{N_f} = \frac{\left(\dot{y}_G^O\right)_{N_f}}{\left(\dot{x}_G^O\right)_{N_f}} \tag{17}$$

and Φ' being the direction of slip on the table. The subsequent curved path of the ball can be shown to describe a parabola, conveniently expressed in the $X'Y'$ coordinate system, which is rotated from XY axes by ψ (see Fig. 6). Where

$$\tan\psi = -\frac{1}{\tan\Phi'_{N_f}} \tag{18}$$

Φ'_{N_f} is obtained from the numerical algorithm explained in Sect. 2.4.3. Expressions for $X_V{}'$ and $Y_V{}'$ have been derived in the detailed analysis of Hopkins and Patterson [27] on the curved path of a bowling ball.

The sliding can be shown to stop at time T_s, given by,

$$T_S = \frac{2s'_{N_f}}{7\mu_s} \tag{19}$$

when the ball is at S (see Fig. 6) or the coordinate $(X_s{}'Y_s{}')$ in the $X'Y'$ system (where s'_{N_f} is the slip velocity of O, on the table, at the termination of impact, obtained at the final iteration of the numerical scheme). Using the derivations of Hopkins and Patterson [27], and also using Eq. (18), it is possible to develop the expressions for $X_s{}'$ and $Y_s{}'$, together with the velocity components $\dot{X}'_S$ and $\dot{Y}'_S$ at the end of the slipping process.

The final velocity at S,

$$V_S = \left(\dot{X}'_S\right)^2 + \left(\dot{Y}'_S\right)^2 \tag{20a}$$

At an angle of θ_S with respect to the XY coordinates, given by,

$$\theta_S = \psi + \lambda = \psi + \tan^{-1}\left(\frac{\dot{Y}'_S}{\dot{X}'_S}\right) \tag{20b}$$

Equations (20a) and (20b) completely define the post-slip motion of the ball, except its sidespin. The sidespin of the ball immediately after impact is also estimated using the numerical algorithm.

The following describes the instantaneous value of sidespin at the end of slip ($t = T_S$),

$$\omega_z^O(t) = \left(\omega_z^O\right)_{N_f} - \dot{\omega}_r t, \text{ if } \left(\omega_z^O\right)_{N_f} > 0 \text{ and } t < \left|\frac{\left(\omega_z^O\right)_{N_f}}{\dot{\omega}_r}\right| \tag{21a}$$

$$\omega_z^O(t) = \left(\omega_z^O\right)_{N_f} + \dot{\omega}_r t, \text{ if } \left(\omega_z^O\right)_{N_f} < 0 \text{ and } t < \left|\frac{\left(\omega_z^O\right)_{N_f}}{\dot{\omega}_r}\right| \tag{21b}$$

$$\omega_z^O(t) = 0, \text{ if } t \geq \left|\frac{\left(\omega_z^O\right)_{N_f}}{\dot{\omega}_r}\right| \tag{21c}$$

$\dot{\omega}_r$ is the resistance of the table to sidespin of the ball, which was measured by the first author to be 22 rad/s^2 for snooker balls [15]. It should also be noted that clockwise rotation of the ball (i.e., right-spin), as seen when looked down at the table, is taken as positive. While the ball is still under the slipping process, its velocity and spin conditions are also available from the work of Hopkins and Patterson [27]. In addition, the ball's sidespin can still be estimated using Eq. (21a).

Table 1 Theoretical predictions, assuming zero sidespin (ω_0^S), and experimental results of ball speeds

Cue ball velocity V_0 (m/s)	Topspin ω_0^T(rad/s)	Cut angle θ (°)	Meas. v_S for cue ball (m/s)	Meas. v_S for object ball (m/s)	Predict. v_S for cue ball (m/s)	Predict. v_S for object ball (m/s)	Error in v_S for cue ball (%)	Error in v_S for object ball (%)
1.539	58.63	33.83	0.816	0.836	0.914	0.831	10.70	–0.62
1.032	39.31	26.36	0.52	0.629	0.520	0.599	–0.03	–5.00
1.364	51.96	40.52	0.925	0.7	0.917	0.676	–0.90	–3.52
1.731	65.94	46.5	1.275	0.787	0.128	0.780	0.18	–0.94
0.942	35.89	18.05	0.365	0.581	0.383	0.579	4.81	–0.38

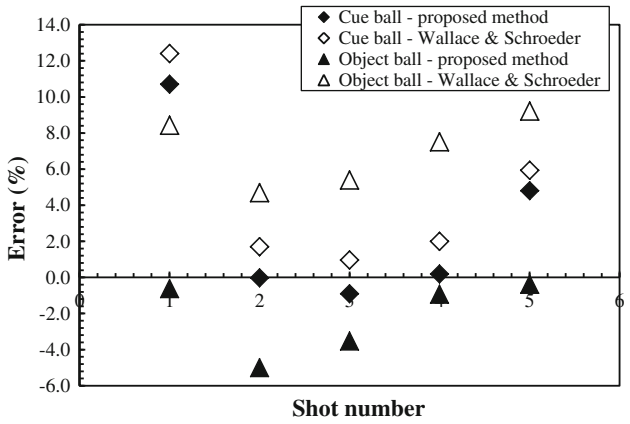

Fig. 7 Comparison of the prediction errors for the five shots for the cue and object ball speeds, V_s, by the proposed method and that of Wallace and Schroeder [20]

3 Results and discussion

Five experimental snooker shots, involving ball collisions, presented in Mathavan et al. [24] are revisited here to check the accuracy obtained through the methodology given in this paper. The authors used an overhead, high speed camera to track the balls with a 1-mm resolution and 0.25-mm accuracy on the table [24]. An experimental procedure was devised, based on the velocity–time plots for the cue ball, before the impacts, with only the shots that had the cue ball rolling before the impacts. Here, the topspin, ω_0^T, is equal to the frontal ball velocity divided by the ball radius, i.e., $\frac{V_0}{R}$. However, the sidespins of the cue ball before the collisions could not be measured [24]. The sidespin values of the cue ball at impact, on the other hand, are considered to be very low as the cue ball was hit on the great circle that is coplanar with the cueing direction as much as possible. Table 1, below, shows the simulated and measured values of the ball velocities at the end of the slipping phase after impacts (i.e., V_S). The data that are used in this section, and the methodology adopted to obtain it, are presented in a greater detail [24].

The five experimental shots, for which the data were presented in Mathavan et al. [24], are also simulated with the impact algorithm presented in this paper. A comparison of the results, presented in Table 1, with that obtained through the predictions of Wallace and Schroeder [20], as given in Mathavan et al. [24], shows that percentile errors are one order lower with the predictions presented in the paper (also seen in Fig. 7). Snooker is a game where the object is not only to pot the object ball, but also to leave the cue ball in a position advantageous for any subsequent shots. So, the post-impact velocity of the cue ball velocity is important in predicting its subsequent position on the table. Hence, from a billiard robot perspective, the algorithm presented in this paper provides a superior ball position predictor for the cue ball.

For the shots given in Table 1, the results of the predicted and measured angles are presented in Table 2. All predicted angles are benchmarked against the measured angles for the five shots. When compared with the predictions that do not consider ball spin [20, 24], the analysis performed in this work reduces the error in the cue ball exit angles by up to six times, as shown in Fig. 8. The error in object ball exit angles is reduced from 9–12 % as presented in Mathavan et al. [24] to just under 5 % as given in Table 2 and Fig. 8. For a realistic billiards simulation, the object ball exit angle is of utmost importance as it directly affects the potting accuracy. The foregoing error reductions in cue and object ball exit angles show that the model incorporating the effects of spin predict the collisions better than the ones that do not take spin into account.

Even though the prediction errors have reduced when compared to methods that do not consider ball spin, a considerable amount of error still remains. In order to quantify the measurement inaccuracies with the experimental procedure, an estimation of the associated errors is performed here. Given that the ball tracking accuracy of the camera system is 0.25 mm, and that the ball collision experiments were performed with 45 frames per second (fps) acquisition [24], the accuracy of velocity measurements is 0.011 m/s. Consequently, for the velocities in the range of 0.94–1.73 m/s, for the five experimental shots, the measurements ambiguities will be in the order of 0.5–1 % with slower shots more prone to the measurement of error. Hence, in the velocity prediction errors of up to ±5 % with

Table 2 Theoretical predictions, assuming zero sidespin (ω_0^S), and experimental results of ball exit angles

Cue ball velocity V_0 (m/s)	Topspin ω_0^T(rad/s)	Cut angle θ (°)	Meas. exit angle for cue ball (°)	Meas. exit angle for object ball (°)	Predict. exit angle for cue ball (°)	Predict. exit angle for object ball (°)	Error in exit angle for cue ball (%)	Error in exit angle for object ball (%)
1.539	58.63	33.83	35.96	33.83	31.93	32.20	–11.21	–4.81
1.032	39.31	26.36	33.20	26.36	32.45	25.07	–2.27	–4.91
1.364	51.96	40.52	30.50	40.51	29.91	38.62	–0.90	–4.67
1.731	65.94	46.5	27.97	46.50	27.32	44.38	–2.34	–4.57
0.942	35.89	18.05	29.86	18.05	29.47	17.15	–1.31	–4.99

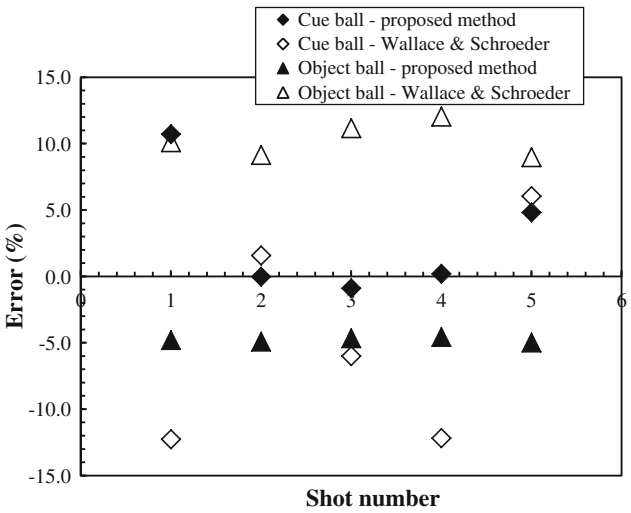

Fig. 8 Comparison of the prediction errors for the five shots for the cue and object ball exit angles by the proposed method and that of Wallace and Schroeder [20]

the proposed method (Fig. 7), a considerable portion must emanate from the theory, mainly from the assumptions made in the form of point contacts and negligible cushion deformations. As far as the angles are considered, at least 4–5 successive ball locations were used to derive the exit angles [24], involving a distance of 150–200 mm, and given the 0.25 mm accuracy of the vision system, the angular errors will be less than 0.1°. Hence, the errors found for the exit angles in Table 2 and Fig. 8 must be solely attributed to the theoretical assumptions made at the start of the paper.

4 Conclusions

This paper provides a comprehensive methodology whereby motion characteristics after a collision between two balls, moving on a plane, can be predicted. The algorithms presented here make use of general theories of dynamics of spheres rolling on a flat surface and general frictional impact dynamics under the assumption of point contacts between the balls under collision and that of the table. Spin dynamics are extensively considered. Finally, quantification is provided for the slipping phases of the ball after impact. Exit velocities and angles immediately after impact, which heavily depend on the spin dynamics, are predicted for the first time and then compared with some experimental shots. The improved prediction accuracies clearly indicate the superiority of this spin model to the current models that do not consider the effects of ball spin on impact. These predictions presented here will be useful for robotic and other virtual systems that are designed to play snooker and billiards, in general.

References

1. World Snooker (2012) http://www.worldsnooker.com/page/NewsArticles/013165~2352434,00.html. Last accessed on the 11th of November 2012 at 19:26 hours (GMT)
2. Coriolis G-G (1835) Théorie Mathémathique des Effets du Jeu de Billard (Carilian-Goeury, Paris, 1835) translated by David Nadler [Mathematical Theory of Spin, Friction, and Collision in the Game of Billiards (David Nadler, USA, 2005)]
3. Salazar A, Sanchez-Lavega A (1990) Motion of a ball on a rough horizontal surface after being struck by a tapering rod. Eur J Phys 11:228–232
4. de la Torre Juárez M (1994) The effect of impulsive forces on a system with friction: the example of the billiard game. Eur J Phys 15(4):184–190
5. Cross R (2005) Bounce of a spinning ball near normal incidence. Am J Phys 73(10):914–992
6. Cross R (2012) Rolling motion of a ball spinning about a near-vertical axis. Phys Teach 50:25–27
7. Long F, Herland J, Tessier M-C, Naulls D, Roth A, Roth G, Greenspan M (2004) Robotic pool: an experiment in automatic potting. In Proceedings of the IROS'04: IEEE/RSJ international conference on intelligent robotics and systems, Sendai, Japan, 3: 2520–2525
8. Ho KHL, Martin T, Baldwin J (2007) Snooker robot player—20 years on. In Proceedings of the IEEE symposium on computational intelligence and games (CIG 2007), Hawaii, 1–5 April 2007:1–8

9. Cheng B-R, Li J-T, Yang, J-S (2004) Design of the neural-fuzzy compensator for a billiard robot. In Proceedings of the 2004 IEEE international conference on networking, sensing and control, Taipei, Taiwan, 21–23 March 2004:909–913
10. Alian ME, Shouraki SE, Shalmani MTM, Karimian P, Sabzmeydani P (2004) Roboshark: a gantry pool player. In Proceedings of the 35th international symposium on robotics (ISR), Paris, France, 2004
11. Jebara T, Eyster C, Weaver J, Starner T, Pentland A (1997) Stochasticks: augmenting the billiards experience with probabilistic vision and wearable computer. In Proceedings of the IEEE international symposium on wearable computers, Cambridge, MA, October 1997:138–145
12. Larsen LB, Jensen MD, Vodzi WK (2012) Multi modal user interaction in an automatic pool trainer. In: Proceedings of the fourth IEEE international conference on multimodal interfaces (ICMI'02), Pittsburgh, USA, pp 361–366, 14–16 October 2002
13. Uchiyama H, Saito H (2007) AR display of visual aids for supporting pool games by online markerless tracking. In Proceedings of the 17th international conference on artificial reality and telexistence (ICAT 2007), Esbjerg, Denmark, 28–30 November 2007: 172–179
14. Hoferlin M, Grundy E, Borgo R, Weiskopf D, Chen M, Griffiths IW, Griffiths W (2010) Video visualization for snooker skill training. Comput Graph Forum 29(3):1053–1062
15. Mathavan S (2009) Trajectory solutions for a game-playing robot using non-prehensile manipulation methods and machine vision. PhD Thesis, Loughborough University, Loughborough, UK
16. Mathavan S, Jackson MR, Parkin RM (2010) A theoretical analysis of billiard ball dynamics under cushion impacts. In: Proceedings of the IMechE, Part C. Journal of Mechanical Engineering Science, vol 224, no 9, pp 1863–1873
17. Nolan A (2006) The development and implementation of an interactive snooker game. Bachelor Degree Thesis, The University of Bath, UK. Last accessed from http://www.cs.bath.ac.uk/~mdv/courses/CM30082/projects.bho/2005-6/nolan-ap-dissertation-2005-6.pdf on the 11 of November 2012 20:19 hours (GMT)
18. Bal B, Dureja G (2012) Hawk eye: a logical innovative technology use in sports for effective decision making. Sport Sci Rev 1–2:107–119
19. Bayes JH, Scott WT (1962) Billiard-ball collision experiment. Am J Phys 3(31):197–200
20. Wallace RE, Schroeder MC (1988) Analysis of billiard ball collisions in two dimensions. Am J Phys 56(9):815–819
21. Marlow WC (1994) The physics of pocket billiards _MAST. Palm Beach Gardens, Florida
22. Kondic L (1999) Dynamics of spherical particles on a surface: collison-induced sliding and other effects. Phys Rev E 60(1):751–770
23. Doménech A (2008) Non-smooth modelling of billiard- and super billiard-ball collisions. Int J Mech Sci 50(4):752–763
24. Mathavan S, Jackson MR, Parkin RM (2009) Application of high-speed imaging in determining the dynamics involved in billiards. Am J Phys 77(9):788–794
25. Stronge WJ (2000) Impact mechanics. Cambridge University Press, Cambridge
26. Kane TR, Levinson DA (1987) An explicit solution of the general two-body collision problem. Comput Mech 2:75–87
27. Hopkins DC, Patterson JD (1977) Bowling frames: paths of a bowling ball. Am J Phys 45:263–266